applied mechanics

Article

Investigation of Working Fluid Performance through a Centrifugal Compression System

James Bull, James M. Buick and Jovana Radulovic *

School of Mechanical and Design Engineering, University of Portsmouth, Portsmouth PO1 3DJ, UK; james.bull@port.ac.uk (J.B.); james.buick@port.ac.uk (J.M.B.)
* Correspondence: jovana.radulovic@port.ac.uk

Abstract: Commonly, researchers have investigated many factors that impact the performance of air conditioning and refrigeration systems, such as varied cooling configurations, operating conditions and optimization of specific system components. Although there is an abundance of research detailing the importance of working fluid selection, very few studies focus on how the working fluid selection influences the performance of the individual components of the system, such as the compressor. In this paper, the performances of a selection of working fluids are compared through a centrifugal compressor using CFD. The working fluids considered are R1234ze, R1234yf, R152a, R444a, R445a, R290 and R600a and were selected due to suitability as replacements to R134a. Each fluid, including R134a, was compared based on the performance of a centrifugal compressor with fixed inlet conditions across two operational speeds. The results indicate that R1234ze and R1234yf demonstrated the best performance as replacements to R134a, achieving the highest overall pressure ratios. Additionally, R1234ze also displayed similar power required through the compressor to R134a indicating greater suitability as a drop-in replacement. The working fluids R444a and R445a both displayed performance similar to that of R134a across both operational speeds, indicating reasonable suitability as a replacement to R134a. Alternatively, R152a, R290 and R600a displayed reduced performance compared to R134a and subsequently, are not suitable replacements based on the compression system considered in this study. As well as considering the observed differences in the performance from the selected working fluids, the implications of the results for industrial applications are also considered, along with avenues for further work.

Keywords: centrifugal compressor; working fluid; CFD

check for updates

Citation: Bull, J.; Buick, J.M.; Radulovic, J. Investigation of Working Fluid Performance through a Centrifugal Compression System. *Appl. Mech.* **2022**, *3*, 815–829. https://doi.org/10.3390/applmech3030048

Received: 30 May 2022
Accepted: 29 June 2022
Published: 2 July 2022

1. Introduction

In the past 12 years, the Earth has experienced 10 of the warmest average annual temperatures since the records began in 1880 [1]. As the temperature of the globe increases, so does the demand for temperature controlling devices such as air conditioning and refrigeration systems. The International Energy Agency (IEA) reported that since 2000, the need for space cooling systems increased by approximately 4% per year [2]. Subsequently, the amount of cooling systems currently operating around the world has grown to 2 billion, and by 2050, this is predicted to increase to 5.6 billion units. Although currently the use of air conditioning and refrigeration systems account for approximately 20% of the total global energy used per day, the predicted growth in demand is expected to result in air conditioning systems becoming the second largest electricity consumer, exceeded only by the industry sector [3]. This raises significant concerns given that in 2019, 84.3% of all energy generation was produced using fossil fuel sources [4]. Subsequently, increasing the energy efficiency of air conditioning and refrigeration systems is of vital importance.

Over the years researchers have investigated many aspects of air conditioning and refrigeration systems such as optimising the design configuration of a cooling system [5–7], improving the performance of the compression system used [8,9] and identifying the

optimal operating conditions [10,11]. However, arguably one of the greatest performance factors of a cooling systems that has been investigated for almost a century is the working fluid selection.

The working fluid choice has the capability to determine the maximum possible performance for any given compression system. Since the 1930s, halocarbon refrigerants were developed and extensively studied for years [12–14]. However, at this time the detrimental effects fluids, such as the chlorofluorocarbons (CFCs) and hydrochlorofluorocarbons (HCFCs), had on the environment were unknown [15,16]. In the 1980s it was identified that the chlorine component of the CFCs and HCFCs was breaking down the ozone layer, therefore the Montreal Protocol was proposed to phase out the use of ozone depleting substances [17,18]. One of the most common CFCs for domestic refrigeration systems, the largest sector of the refrigeration industry, was that of R12. To phase out R12, research conducted comparisons based on fluids with similar thermodynamic properties. Over the years there have been substantial research supporting R134a as an ideal replacement for R12 [19–21]. In accordance with the EU 517/2014 regulations [22], limits on Global Warming Potential (GWP) direct researchers to adapt and consider alternative working fluids within refrigeration systems. The specific limit of GWP is dependent on the application. For domestic systems, a GWP of less than 150 is stated as a suitable reference value. Therefore, previously used refrigerants, such as R134a, are required to be phased out and investigations over the years have focused on identifying suitable replacements.

Bolaji [23] investigated the notion of using R152a and R32 as suitable replacements for R134a in a domestic refrigeration system. Based on operating conditions, the required design temperature of −3 °C was achieved quicker in the cycles using R152a and R134a than R32. Additionally, R152a had the lowest power consumption through the compression stage and achieved a Coefficient of Performance (COP) value 4.7% higher than that of R134a. Whereas in comparison, R32 achieved a COP 8.5% lower than R134a and had the highest discharge temperature. It was concluded based on the two fluids compared with R134a, R152a could be used as a suitable replacement.

Another fluid investigated as an alternative to R134a is R600a, which was originally proposed as a replacement to R12 [20,24]. Joybari et al. [25] conducted an exergy analysis of R600a as a replacement to R134a in a domestic refrigeration system finding that the exergy destruction is 45.05% less using R600a compared to R134a.

Aprea et al. [26] conducted a study using R1234ze as a drop-in replacement for R134a given the extremely low GWP value of 6 for R1234ze [27]. It was identified that the average power required for the refrigeration system was 9% lower using R1234ze. Additionally, R1234ze has a lower environmental impact when considering the direct and indirect emissions related to the entire refrigerant lifespan.

In 2011, Zilio et al. [28] looked at the possibility of using R1234yf within an automotive air conditioning system designed for R134a. Using a drop-in system, the cooling capacity and COP of the cycle was reduced by 12–24% and 2–19%, respectively when using R1234yf instead of R134a. However, it was suggested that by making slight modifications to the cycle set up R1234yf could achieve higher COP values at the same cooling capacity as R134a.

The option of using R1234yf as a drop-in replacement for R134a within a vapor compression system has also been considered. In 2013 Navarro-Esbri et al. [29] compared the performance R1234yf and R134a by varying condensing pressure and evaporating pressure. It was identified that the cooling capacity of R1234yf was approximately 9% lower than that of R134a across the operational range. However, as the condensing temperature increased, the difference in cooling capacity decreased. It was also identified that the COP values obtained for R1234yf were between 5–30% lower than R134a. When the condensing temperature was raised from 313.15 K to 333.15 K the range of COP value decreased from 25% to 8%. It was concluded that the experimental results indicate that R1234yf can be a suitable drop-in replacement for R134a at higher condensing temperatures.

Sanchez et al. [30] expanded the alternative working fluid choice for R134a to include R1234ze, R600a, R290, R152a and R1234yf. All fluids were tested across two evaporating

temperatures of 263.15 K and 273.15 K and three condensing temperatures of 298.15 K, 308.15 K and 318.15 K. It was identified that R290 presented the best increase for cooling capacity and COP of 40.5–67.4% and 2.8–22.4%, respectively. However, it required up to 44.8% more power for the compressor. R152a was found to have a decrease in both cooling capacity and power required of 4.5% and 8.6%, respectively. Interestingly, due to the reduction in power, the COP increase by 1–4.8%. Similar to previous findings [28,29], R1234yf had a slight decrease in both cooling capacity and COP of approximately 7% and 10%, respectively. It was also reported that both R1234ze and R600a had a significant decrease in cooling capacity and power requirement. It is noted that to achieve a similar cooling capacity to R134a, R1234ze and R600a require a compressor with a larger displacement.

Mota-Baboloni et al. [31] presented the possibility of using a refrigerant mixture as a suitable R134a replacement. Out of the 7 proposed mixtures, only R444a demonstrated overall improvements to COP and cooling capacity. Devecioğlu and Oruç [32] further supported this by comparing the performance of R1234yf, R444a and R445a in an air conditioning system. The fluids were tested with evaporation temperatures of 268.15 K and 278.15 K and condensation temperatures of 303.15 K and 333.15 K. It was identified that both R444a and R445a had lower COP than R1234yf but increased cooling capacity. If maximizing COP is not the main objective, both R444a and R445a are adequate replacements for R134a.

Other studies also investigated the performance of alternative working fluids to R134a within a refrigeration cycle [33]. The main findings indicate that for a specific cooling capacity, both R1234ze and R1234yf required less work done through the compressor and simultaneously achieved greater COP than R134a. Alternatively, in a cycle with fixed work done by the compressor, the fluid mixtures R444a and R445a achieved greater cooling capacity and COP.

From the research discussed above, it is clear that the working fluid choice for a cooling system depends on many factors such as the application, system configuration or operating conditions. However, a limitation in studies of this nature is that the performance of a working fluid often assumes fixed details for the components within the system such as the efficiency of the compressor. Therefore, in this present study we investigate a comparison of working fluids based upon performance through an existing centrifugal compressor design at fixed inlet conditions. The main premise is to evaluate how the performance of the compressor varies with alternative working fluids as a direct drop-in replacement to R134a.

The working fluids considered for comparison are R1234ze, R1234yf, R134a, R600a, R152a, R290, R444a and R445a. These fluids were selected based on their common use as replacements for R134a. The GWP, Ozone Depletion Potential (ODP) and safety classification of the working fluids are given in Table 1. All fluids studied have low toxicity; however, R600a and R290 are highly flammable and R1234ze, R1234yf, R444a and R445a are mildly flammable.

Table 1. Summary of working fluids discussed with properties. Data retrieved from RefProp [27].

Refrigerant	GWP	ODP	Safety Classification
R134a	1430	0	A1
R152a	124	0	A2
R600a	3	0	A3
R290	3.3	0	A3
R1234ze	6	0	A2L
R1234yf	4	0	A2L
R444a	93	1	A2L
R445a	146	1	A2L

2. Materials and Methods

The impeller blade geometry was created within DesignModeller based upon the model used within [34] without a splitter blade. Figure 1a and 1b demonstrate the impeller blade geometry and corresponding meridional view used within this section, respectively.

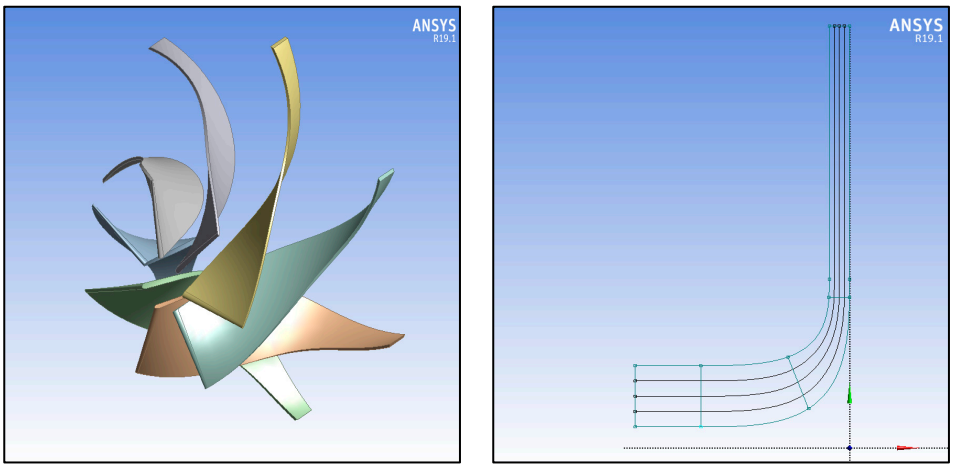

(**a**) (**b**)

Figure 1. Impeller Blade Design (**a**) and Meridional Plane View (**b**).

The pre-impeller, impeller and diffuser domains are shown in Figure 2, respectively. In order to simulate the rotation imparted on the fluid through the impeller, the impeller domain is set to a rotating component type and the pre-impeller and diffuser domain set to stationary. The wall configuration on the shroud side of the impeller domain is set at a counter rotating velocity to ensure the hub wall in the impeller rotates and shroud wall is stationary.

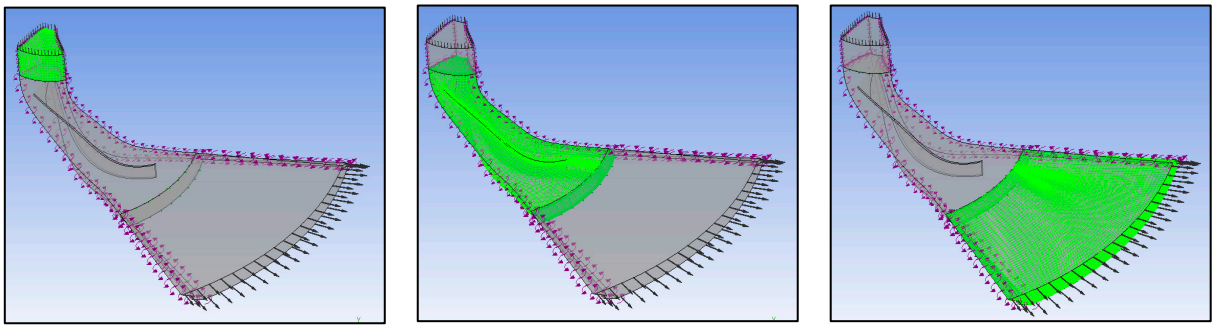

(**a**) (**b**) (**c**)

Figure 2. Domain Setup Highlighting the Pre-Impeller (**a**), Impeller (**b**) and Diffuser (**c**).

Figure 3 highlights the main specified interfaces where all other boundaries are defined as no slip walls and assumed smooth. The inlet and outlet boundaries shown in Figure 3a are specified as a total pressure/total temperature inlet and mass flow rate outlet, respectively. To conserve mesh size and computational requirement, a 7th of the blade is simulated and periodic boundaries, shown in Figure 3b, are used. Figure 3c highlights the interface between the pre-impeller to impeller and impeller to diffuser domains.

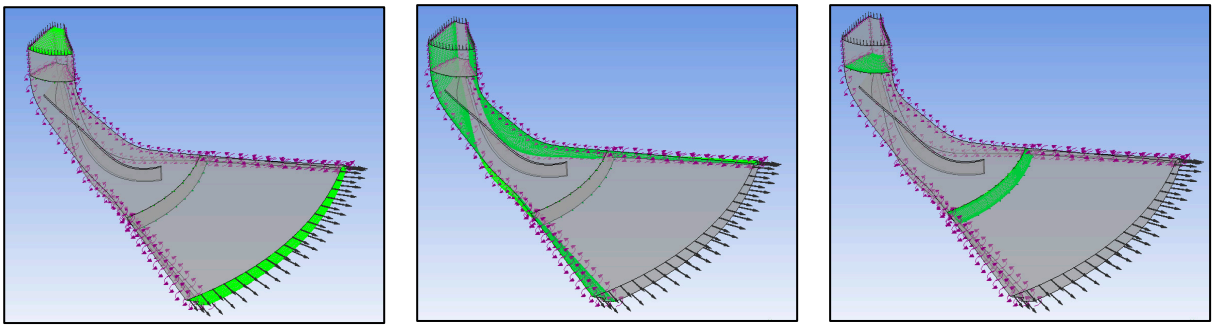

(**a**) (**b**) (**c**)

Figure 3. Defined Interfaces for the Inlet and Outlet (**a**), Periodic Boundaries (**b**) and Frozen Rotor Frame Change from the Inlet to Impeller and Impeller to Outlet (**c**).

The frozen rotor model was used between the pre-impeller to impeller and impeller to diffuser interface.

The generated impeller blade was meshed using TurboGrid. The overall mesh size was defined by the global size factor with first element offset for boundary layer refinement control and additional target maximum expansion rate enabled. The passage spanwise blade distribution parameters were set to use the proportional method with a factor of 1. The hub tip and shroud tip distribution parameters were both fixed with the match expansion at blade tip control. The inlet used a H-Grid mesh type defined by a target number of elements to ensure a suitable mesh density leading to the inlet of the impeller. The outlet also uses the H-Grid mesh type, but it was defined by a target expansion rate. A mesh convergence was carried out by adjusting the global size factor setting.

Figure 4a shows a global base size of 1 provides a sufficient element count for ascertaining the pressure ratio achieved and Figure 4b shows the corresponding mesh view of the simplified impeller geometry with a global base size of 1, which was used in the subsequent simulations. The CFD model was tested and validated against experimental results as shown within [34]. The fluid was modelled using the K-Omega SST turbulence model proposed by Menter [35]. This model was selected due to the consistent performance throughout all domains of a centrifugal compressor compared to other turbulence models [36].

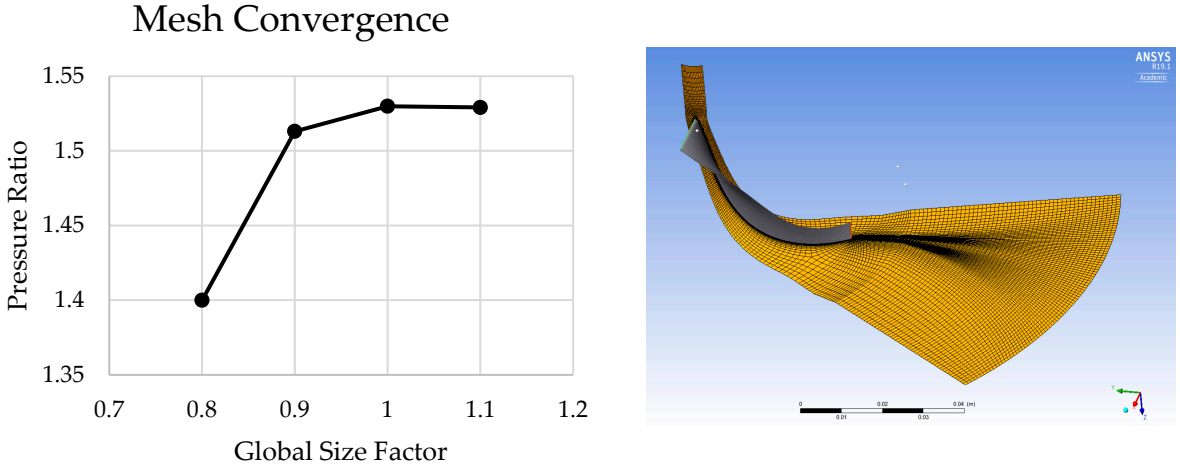

(**a**) (**b**)

Figure 4. Mesh Convergence of Impeller Geometry (**a**) and Meshed Impeller Blade with Global Size Factor of 1 (**b**).

Fluid Definition

The fluid is modelled as a real gas using the Peng–Robinson Equation of State show in Equation (1). With a, b, α, k and T_r calculated by Equations (2)–(6), respectively.

$$p = \frac{RT}{V_m - b} - \frac{a\alpha}{V_m^2 + 2bV_m - b^2} \quad (1)$$

$$a = 0.45724\frac{R^2T_c^2}{p_c} \quad (2)$$

$$b = 0.0778\frac{RT_c}{p_c} \quad (3)$$

$$\alpha = \left(1 + k\left(1 - T_r^{\frac{1}{2}}\right)\right)^2 \quad (4)$$

$$k = 0.37464 + 1.54227\omega - 0.26992\omega^2 \quad (5)$$

$$T_r = \frac{T}{T_c} \quad (6)$$

where p is pressure, R is the universal gas constant, T is temperature, V_m is molar volume, ω. is acentric factor and subscript c is the critical point value of the fluid.

The specific heat capacity of the fluid is calculated based on the zero-pressure polynomial option shown in Equation (7).

$$\frac{C_{p0}}{R} = a_1 + a_2T + a_3T^2 + a_4T^3 + a_5T^4. \quad (7)$$

where R is the universal gas constant, T is temperature and the coefficients, a_i, are retrieved from RefProp. The reference state of the working fluid was taken as the saturated vapor fluid properties at the inlet pressure. Table 2 demonstrates the fluid properties used in the simulation set up for each working fluid retrieved from RefProp [27]. As R444a and R445a are predefined mixtures of pure fluids based on mass percentage shown in Table 3.

Table 2. Fluid Properties.

Fluid	Critical Point				Acentric Factor	Boiling Temperature (K)	Molar Mass (kg/kmol)	Specific Gas Constant (J/kg-K)
	Temperature (K)	Pressure (MPa)	Density (kg/m^3)	Volume (cm^3/mol)				
R1234ze	382.51	3.63	540.84	210.86	0.31	254.18	114.04	0.07
R134a	374.21	4.06	511.9	199.32	0.33	247.08	102.03	0.08
R1234yf	367.85	3.38	475.55	239.81	0.28	243.67	114.04	0.07
R152a	386.41	4.52	368	179.49	0.28	249.13	66.05	0.13
R290	369.89	4.25	220.48	200	0.15	231.04	44.1	0.19
R600a	407.81	3.63	225.5	257.75	0.18	261.4	58.12	0.14
R32	351.26	5.78	424	122.7	0.28	221.5	52.02	0.16
CO2	304.13	7.38	467.6	94.12	0.22	194.69	44.01	0.19

Table 3. Mass Percentage Composition of R444a and R445a.

Fluid Mixture	Fluid	Mass (%)
R444a	R32	12
	R152a	5
	R1234ze	83
R445a	CO_2	6
	R134a	9
	R1234ze	85

The inlet pressure was set as the saturated vapor pressure at 273.15 K with inlet temperature at 5 K superheat. The RPMs considered for the impeller blade were consistent across all fluids to ensure viable comparison of the power required for the compression stage. Each fluid was simulated at an RPM of 35,000 and 40,000, which were determined based on capabilities of the impeller design and volume flow rate of 0.05 m^3/s. Table 4 demonstrates the inlet conditions specified for each fluid.

Table 4. Inlet Conditions for Working Fluids Simulated.

Fluid	Temperature (K)	Pressure (MPa)	Inlet Density (kg/m^3)	Mass Flow Rate (kg/s)
R1234ze	278.15	0.21655	11.446	0.5723
R1234yf	278.15	0.31582	17.194	0.8597
R152a	278.15	0.26399	8.1573	0.4079
R134a	278.15	0.29280	14.066	0.7033
R444a	278.15	0.27561	12.438	0.6219
R445a	278.15	0.26065	12.446	0.6223
R290	278.15	0.47446	10.085	0.5043
R600a	278.15	0.15696	4.1652	0.2083

In order to evaluate the performance of the working fluid, the power required, output temperature and output pressure were recorded from the simulations. The output temperature and pressure were taken as the surface average values at the outlet of the diffuser domain. The power required for a given working fluid, P, was calculated as a function of the angular velocity of the impeller, Ω, the number of impeller blades, n, and the torque experienced by a single blade, τ, as shown in Equation (8).

$$P = \Omega n \tau \tag{8}$$

An additional variable used to compare the performance of the working fluids was the pressure ratio achieved per specific work done. This was calculated based on the mechanical work applied by the compressor and gives a ratio between the pressure ratio achieved and power required, based on 1 kg of fluid and is defined by Equation (9).

$$\text{Pressure Ratio Per Specific Work Done} = \frac{p_r \dot{m}}{P} \tag{9}$$

where p_r is pressure ratio achieved and $\dot{m}$ is the mass flow rate for a specific fluid.

3. Results/Discussion

The pressure contours for R1234ze, R1234yf, R152a, R134a, R444a, R445a, R290 and R600a can be seen in Figures 5–12, respectively. For all fluids increasing the RPM from 35,000 to 40,000 resulted in increased pressure ratio at the outlet of the diffuser. In general, as the fluid enters the impeller blade passage, the pressure demonstrated minimal increase to approximately 50–60% of the impeller passage meridional length. Then, as the fluid flows towards the trailing edge of the impeller blade, the pressure increases more rapidly, with pressure increase being higher on the pressure side of the impeller blade compared to the suction side. When exiting the impeller passage and entering the diffuser domain, the fluid starts to decelerate as the cross-sectional area of the diffuser increases, thus achieving maximum pressure at the outlet of the diffuser.

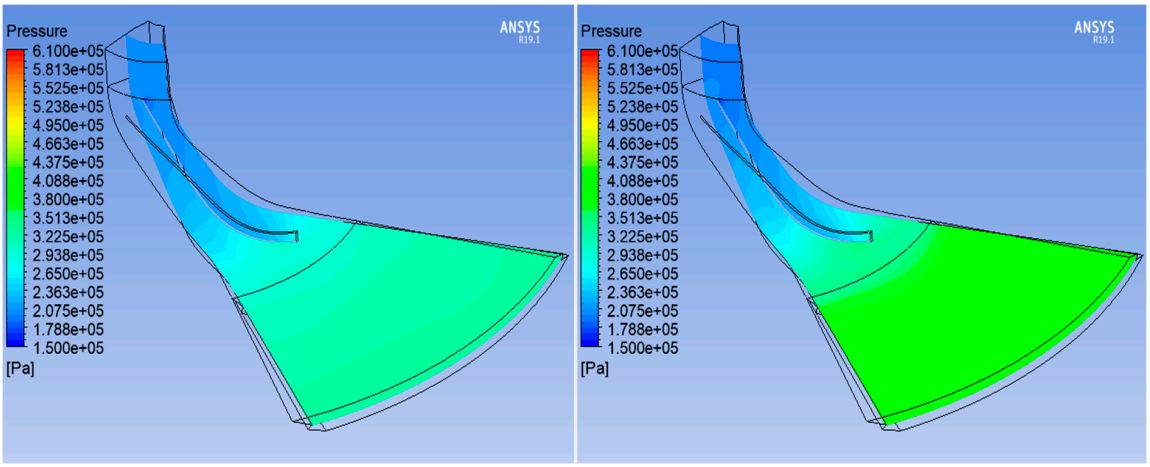

(**a**) (**b**)

Figure 5. Pressure Contour for R1234ze at an RPM of 35,000 (**a**) and 40,000 (**b**).

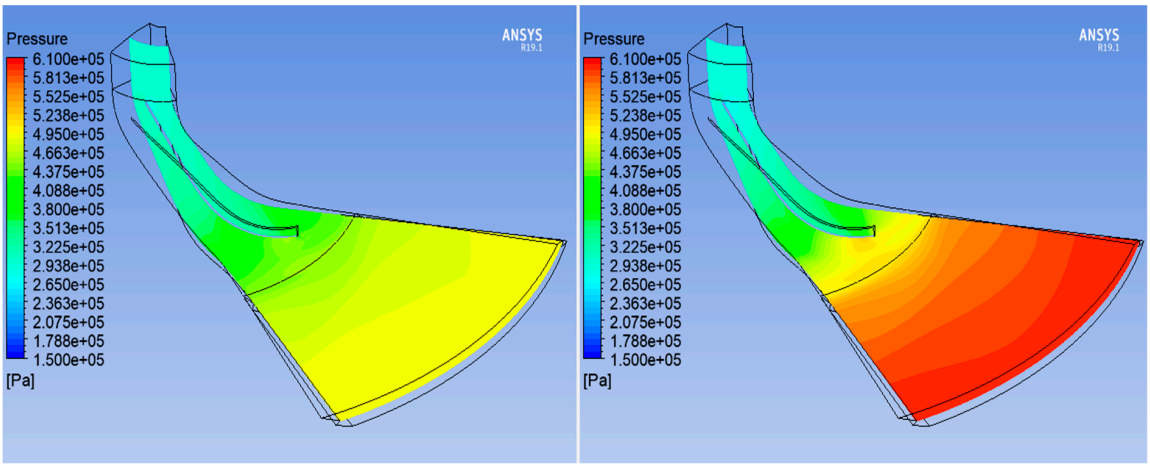

(**a**) (**b**)

Figure 6. Pressure Contour for R1234yf at an RPM of 35,000 (**a**) and 40,000 (**b**).

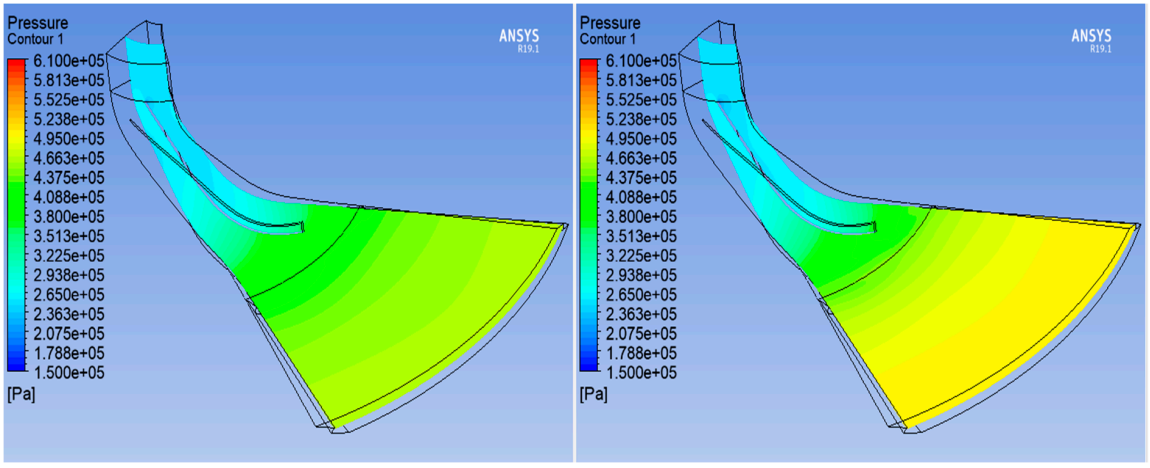

(**a**) (**b**)

Figure 7. Pressure Contour for R152a at an RPM of 35,000 (**a**) and 40,000 (**b**).

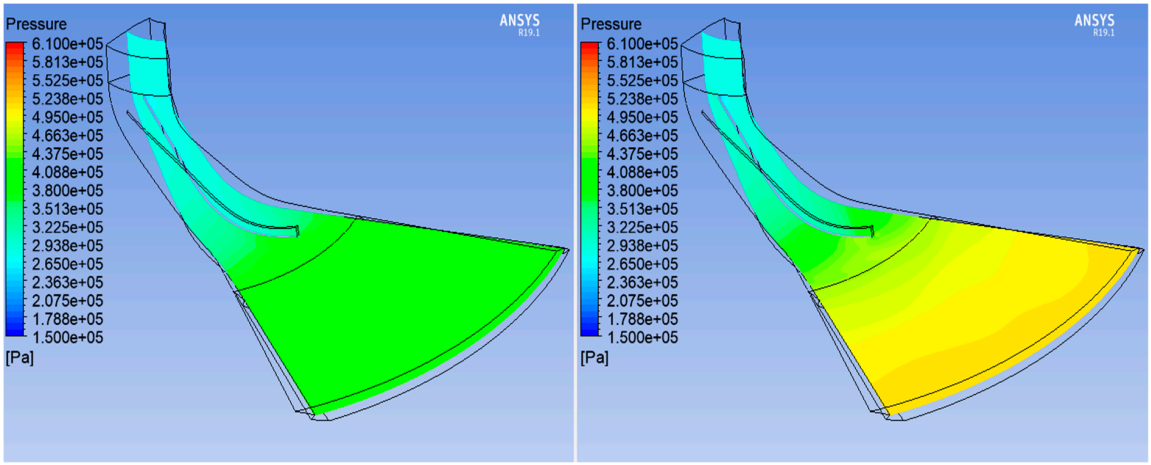

(**a**) (**b**)

Figure 8. Pressure Contour for R134a at an RPM of 35,000 (**a**) and 40,000 (**b**).

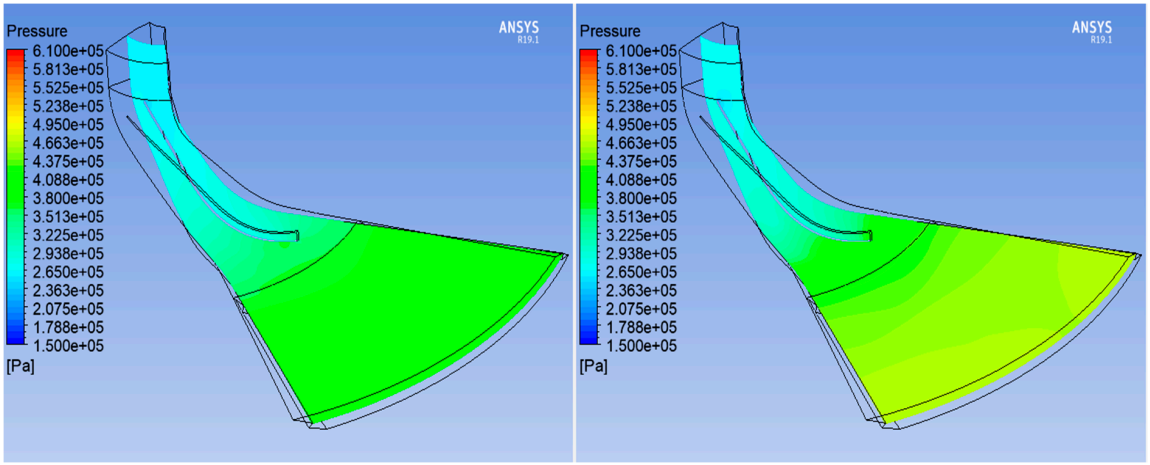

(**a**) (**b**)

Figure 9. Pressure Contour for R444a at an RPM of 35,000 (**a**) and 40,000 (**b**).

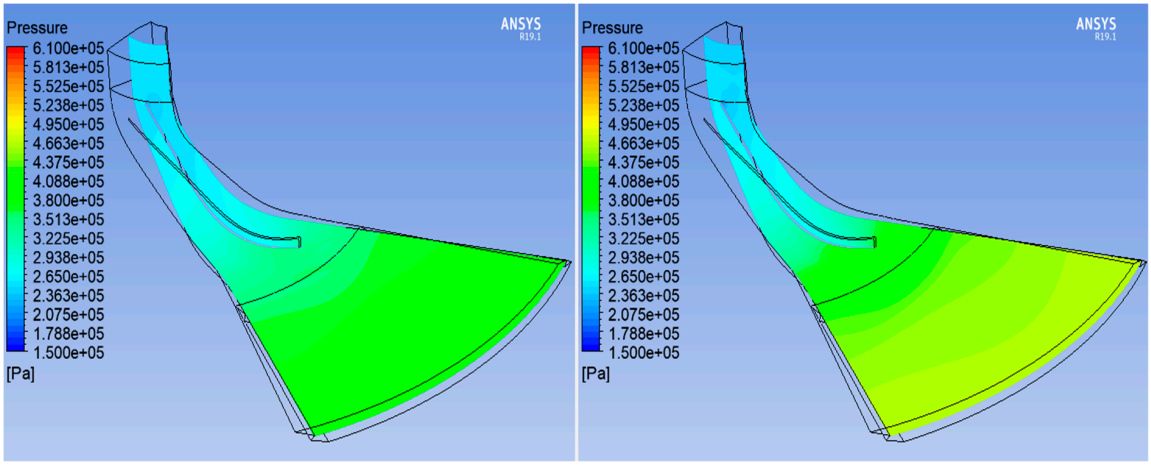

(**a**) (**b**)

Figure 10. Pressure Contour for R445a at an RPM of 35,000 (**a**) and 40,000 (**b**).

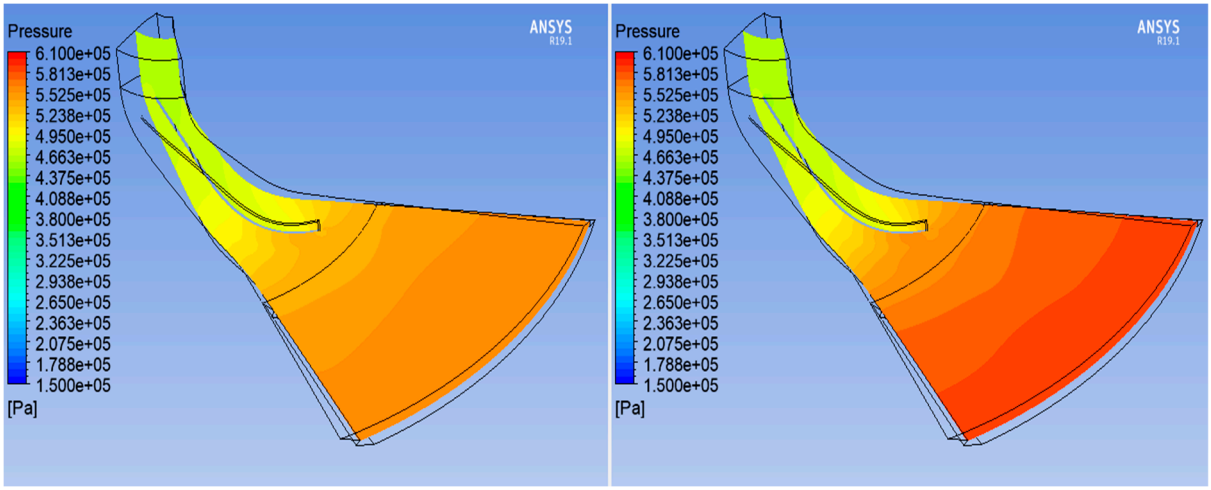

(**a**) (**b**)

Figure 11. Pressure Contour for R290 at an RPM of 35,000 (**a**) and 40,000 (**b**).

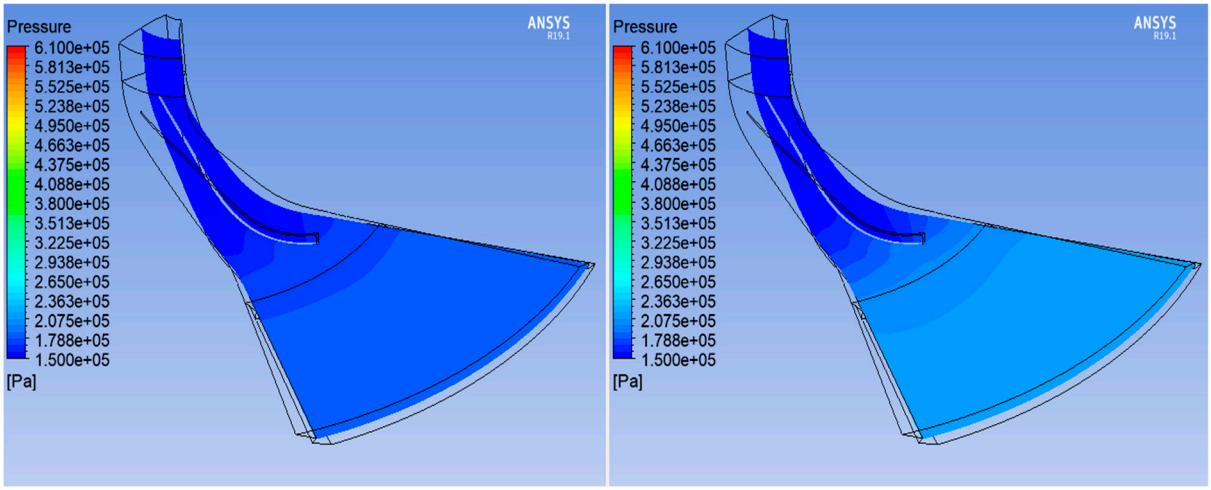

(**a**) (**b**)

Figure 12. Pressure Contour for R600a at an RPM of 35,000 (**a**) and 40,000 (**b**).

Figure 13 displays a comparison of the pressure ratio achieved at 35,000 and 40,000 RPM. R1234yf demonstrated the highest-pressure ratios of 1.58 and 1.93 for both 35,000 and 40,000 RPM, respectively, closely followed by R1234ze with pressure ratios of 1.52 and 1.88 at the respective impeller speeds. This indicates both R1234ze and R1234yf would require a lower operational speed to achieve a similar pressure ratio, thus reducing the power requirements.

R152a and R445a displayed similar pressure ratios at 35,000 RPM with values of 1.47 and 1.48, respectively. Likewise, R134a and R444a also displayed comparable pressure ratios at 35,000 RPM of 1.43 and 1.44, respectively. Furthermore, at 40,000 RPM R152a and R134a achieved similar pressure ratios of approximately 1.78.

R444a achieved pressure ratios lower than that of R1234ze and R152a at both RPMs. Given that R1234ze and R152a are two of the fluids that make the composition of R444a, this suggests fluid properties related to the fluid mixture composition impact the pressure ratio achieved. Specifically, the influence R32 has on the overall properties of R444a decreases the pressure ratio.

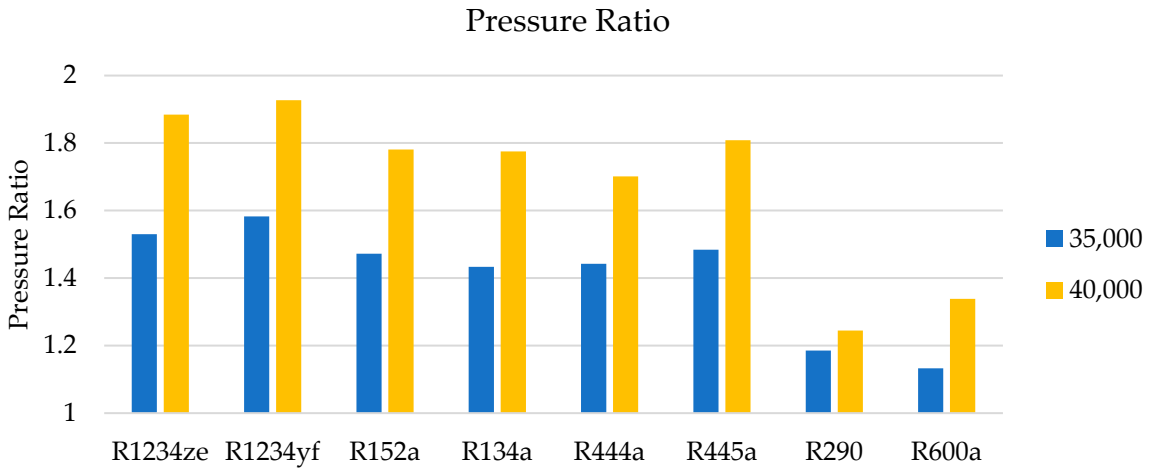

Figure 13. Comparison of Pressure Ratio Achieved for each Working Fluid at an RPM of 35,000 and 40,000.

The lowest pressure ratios were achieved by R290 and R600a. R600a had the lowest value at 35,000 RPM with 1.13 and R290 had lowest value at 40,000 RPM with 1.24. Virtually all fluids showed an increase in the pressure ratio in the range of 18–24% when the speed was increase from 35,000 to 40,000 RPM. The exception being R290, which demonstrated only a 5% increase in pressure ratio between 35,000 and 40,000 RPM R290.

Figure 14 demonstrates the absolute outlet pressure recorded at the two RPMs considered. Despite the lower pressure ratios (showed in Figure 13), R290 had the highest and second highest outlet pressure at 35,000 and 40,000 RPM, respectively. This can be attributed to the absolute inlet pressure of 0.47446 MPa which is higher that the outlet pressure for the majority of fluids, with the exception of R134a at 40,000 RPM and R1234yf at both rotational speeds.

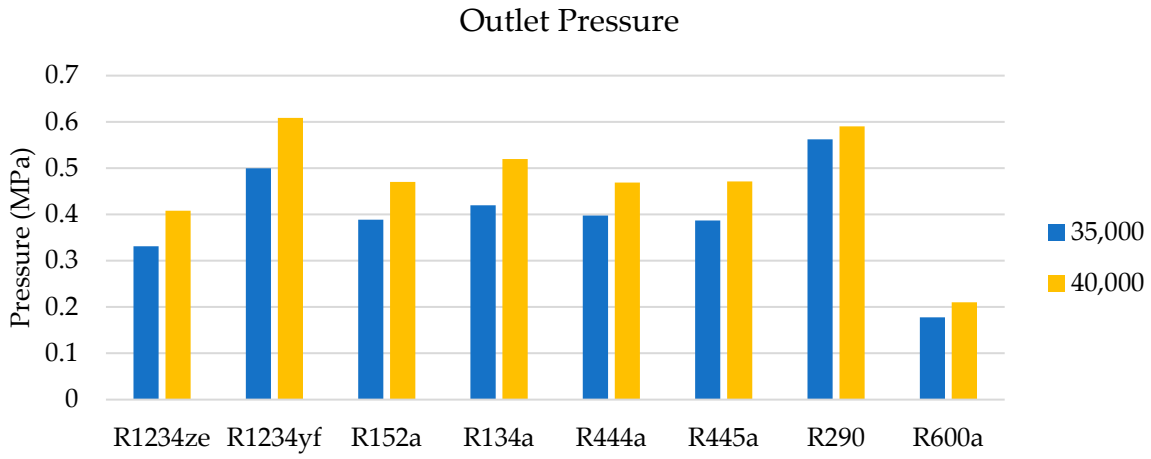

Figure 14. Comparison of Outlet Pressure Achieved for each Working Fluid at an RPM of 35,000 and 40,000.

R152a, R444a and R445a demonstrated similar outlet pressures at both 35,000 and 40,000 RPM with values in the range 0.38683–0.39748 MPa and 0.46878–0.47133 MPa, for the two speeds, respectively. Considering the initial conditions displayed in Table 4, R152a, R444a and R445a all have similar absolute inlet pressures of 0.26399 MPa, 0.27561 MPa and 0.26065 MPa, respectively. Therefore, the similarities in the inlet pressures and relevant fluid properties are reflected in the similarities in outlet pressure.

Despite achieving the second highest pressure ratios, R1234ze achieved the second lowest outlet pressure with 0.33129 MPa and 0.40799 MPa at 35,000 and 40,000 RPM,

respectively. R600a achieved the lowest outlet pressure at both 35,000 and 40,000 RPM with values of 0.17772 MPa and 0.21008 MPa, respectively.

Figure 15 demonstrates a comparison of the power required for each working fluid at 35,000 and 40,000 RPM. R1234yf displayed the highest compressor power required at both 35,000 and 40,000 RPM with values of 2.17 kW and 3.3 kW, respectively. R1234ze, R134a and R445a achieved similar compressor power required at 40,000 RPM of 2.14 kW, 2.16 kW and 2.15 kW, respectively. As R1234ze and R445a also achieved higher pressure ratio than R134a, this indicates that R1234ze and R445a achieve greater performance than R134a with approximately the same power. Furthermore, at 35,000 RPM R1234ze required less power than R134a, agreeing with previous findings [26]. Additionally, R152a required less power than R134a at both 35,000 and 40,000 and achieved similar pressure ratio as displayed in Figure 13. This further agrees with previous findings that R152a could be used as a replacement to R134a [23,30].

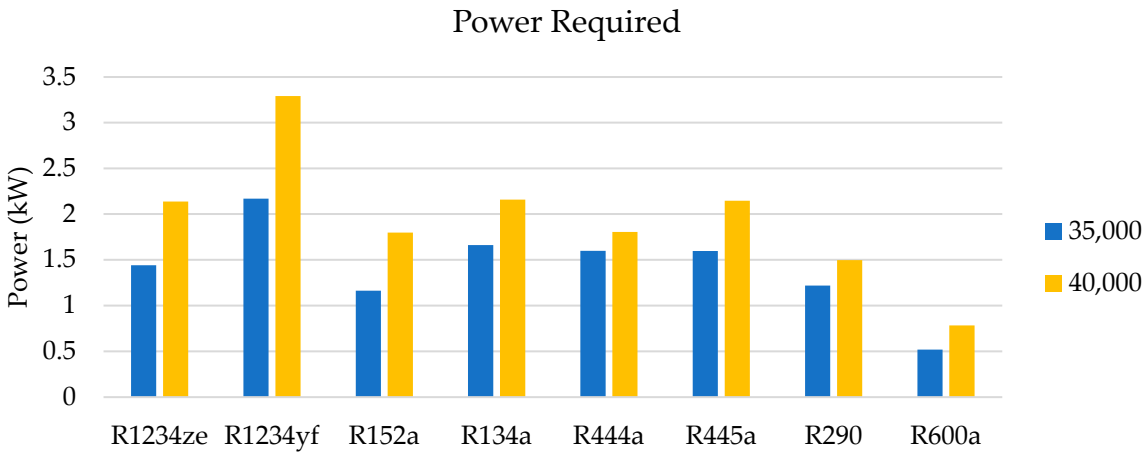

Figure 15. Comparison of Power Required for each Working Fluid at an RPM of 35,000 and 40,000.

R600a demonstrated the lowest power required through the compressor for both 35,000 and 40,000 RPM with values of 0.52 kW and 0.78 kW, respectively, which is in line with the lowest pressure ratio produced. Similarities can also be noted with R444a and R445a that displayed comparable power requirements for 35,000 RPM at approximately 1.6 kW. However, at 40,000 RPM, R444a required 0.34 kW less than R445a.

Figure 16 compares pressure ratio per specific work done by the compressor based on 1 kg of working fluid. Considering the rotational speed of 35,000 RPM, R1234yf demonstrated the highest overall pressure ratio per specific work done with a value of 0.627 kJ^{-1}, closely followed by R1234ze and R134a with values of 0.608 kJ^{-1} and 0.606 kJ^{-1}, respectively, showing a favorable greater pressure ratio achieved per power required at this speed compared to the other fluids. Considering a rotational speed of 40,000, R444a displayed highest pressure ratio to specific work done with a value of 0.586 kJ^{-1}. R134a achieved the second highest value of 0.578 kJ^{-1}. For both 35,000 and 40,000 RPM, R600a demonstrated the lowest pressure ratio per specific work values of 0.455 kJ^{-1} and 0.356 kJ^{-1}, respectively.

Most fluids, with the exception of R444a, showed higher pressure ratio per specific work done at 35,000 RPM compared to 40,000 RPM presented in Table 5. R1234yf, R152a and R600a displayed the largest decrease of −19.73%, −21.76% and −21.85%, respectively.

In contrast, R134a and R444a demonstrated the smallest percentage difference of −4.62% and 4.45%, respectively. R134a and R444a have a more consistent performance across the operational speeds considered compared to the other working fluids. R444a shows an increase in pressure ratio per specific work done of the compressor, indicating greater utilization of power to pressure ratio achieved at a higher RPM.

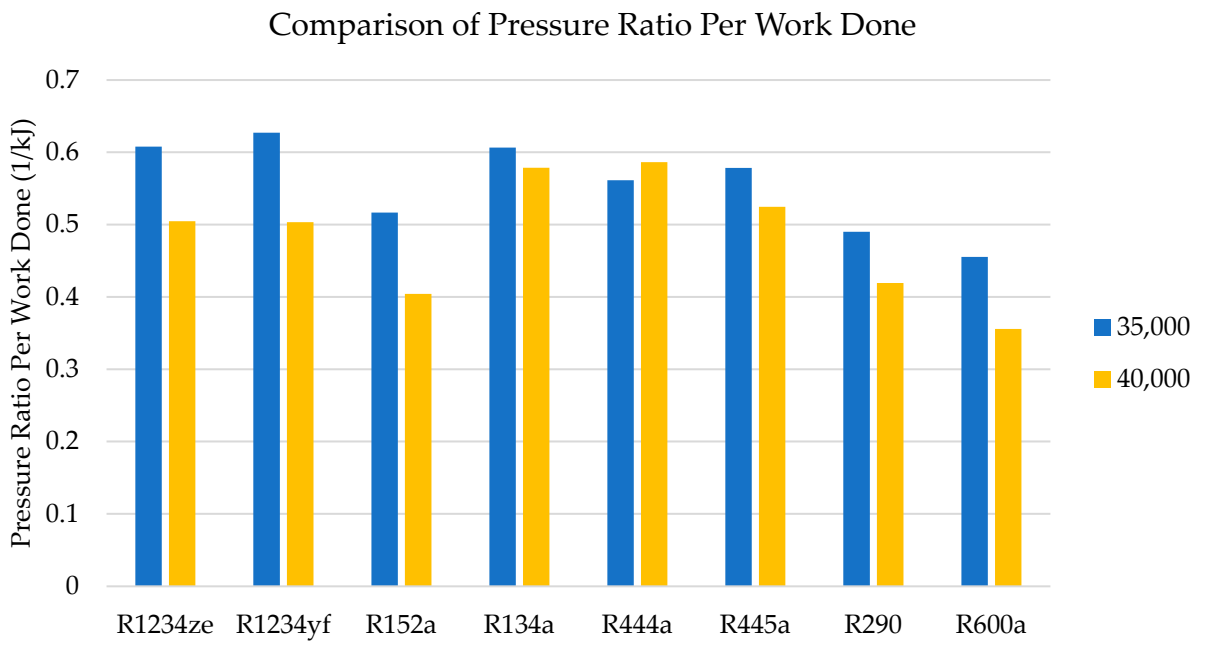

Figure 16. Comparison of Pressure Ratio Increase Per Specific Work Done by the Compressor Based on 1 kg of Fluid.

Table 5. Pressure Ratio Increase Per Specific Work Done by the Compressor Based on 1 kg of Fluid.

Fluid	RPM		Difference (%)
	35,000	40,000	
R1234ze	0.608	0.505	−16.97%
R1234yf	0.627	0.503	−19.73%
R152a	0.517	0.404	−21.76%
R134a	0.606	0.578	−4.62%
R444a	0.561	0.586	4.45%
R445a	0.578	0.525	−9.28%
R290	0.49	0.419	−14.45%
R600a	0.455	0.356	−21.85%

4. Conclusions

Based the results presented and analyzed within this paper utilizing different working fluid alternatives as drop-in replacements to R134a through a centrifugal compressor design can adjust the performance of the compression stage. Regarding the working fluid comparisons based on the performance of the centrifugal compressor, the following conclusions can be made:

1. R1234yf and R1234ze achieved highest pressure ratio across both 35,000 and 40,000 RPM. However, R1234yf required the highest compressor power out while R1234ze required power similar to that of R134a highlighting R1234ze as a more suitable drop-in replacement for R134a.
2. R444a and R445a both achieved similar performance to that of R134a especially in terms of power required through the compressor stage. R444a displayed the closest result when considering the pressure ratio achieved per specific work done by the compressor, whereas R445a displayed the closest absolute power required though the compression system.
3. Although R152a achieved pressure ratios similar to R134a utilizing less power, the pressure ratio per specific work done was lower than all fluids with the exception of R600a and R290 that displayed the lowest.

4. Despite displaying the lowest powers required through the compressor than most other fluids, R600a also achieved the lowest pressure ratios. R600a additionally demonstrated the lowest pressure ratio per specific work done by the compressor.
5. R290 also displayed lower pressure ratios across both speeds compared to the other fluids considered.

From an industrial perspective, these findings provide an insight into the effect on compressor operation of working fluid replacement. The results indicate that R1234ze, R1234yf, R444a and R445a would be suitable as replacements to R134a. Furthermore, it was also identified that R1234ze and R1234yf could achieve pressure ratios similar to R134a in a compression system with lower operational speed. By reducing the operational speed of the system, not only would the power requirement decrease, but there would be reduced forces and wear on compression system components, such as the bearings.

This research will assist industry in making the transformation to more environmentally friendly working fluids within existing compressor systems. It has highlighted the performance of a range of commonly considered alternative working fluids in terms of the power requirements, the achieved pressure and the pressure ratio increase per unit of specific work done. This will enable the associated environmental advantages of these working fluids to be achieved in existing systems, while also highlighting the efficiency of the compressor which is also important from an environmental point of view.

Further work should be conducted to investigate how the differences observed in fluid performance through a compression system relate to the performance of a cooling system. Specifically, whether improved compressor performance of a fluid translates to the measured performance variables of a cooling system, such as (COP) and cooling capacity.

Author Contributions: Conceptualization, J.B., J.M.B. and J.R.; methodology, J.B., J.M.B. and J.R.; software, J.B.; validation, J.B.; formal analysis, J.B., J.M.B. and J.R.; investigation, J.B., J.M.B. and J.R.; resources, J.B.; data curation, J.B., J.M.B. and J.R.; writing—original draft preparation, J.B.; writing—review and editing, J.B., J.M.B. and J.R.; visualization, J.B.; supervision, J.M.B. and J.R.; project administration, J.M.B. and J.R.; funding acquisition, J.M.B. and J.R. All authors have read and agreed to the published version of the manuscript.

Funding: J.B. gratefully acknowledges funding through a PhD bursary from Business Edge Limited and the University of Portsmouth.

Institutional Review Board Statement: Not applicable.

Informed Consent Statement: Not applicable.

Data Availability Statement: The data presented in this study are available on request from the corresponding author.

Conflicts of Interest: The authors declare no conflict of interest.

References

1. NOAA. *NOAA National Centers for Environmental Information, State of the Climate: Global Climate Report for 2021*; NOAA: Washington, DC, USA, 2022.
2. IEA. *Cooling*; IEA: Paris, France, 2021.
3. IEA. *The Future of Cooling*; IEA: Paris, France, 2018.
4. Hannah Ritchie, M.R.; Rosado, P. Energy. Our World in Data. 2020.
5. Tahmasebzadehbaie, M.; Sayyaadi, H. Optimal design of a two-stage refrigeration cycle for natural gas pre-cooling in a gas refinery considering the best allocation of refrigerant. *Energy Convers. Manag.* **2020**, *210*, 112743. [CrossRef]
6. Saleh, B.; Aly, A.A.; Alsehli, M.; Elfasakhany, A.; Bassuoni, M.M. Performance Analysis and Working Fluid Selection for Single and Two Stages Vapor Compression Refrigeration Cycles. *Processes* **2020**, *8*, 1017. [CrossRef]
7. Wang, Q.; Li, T.; Jia, Y.; Zhang, W. Thermodynamic performance comparison of series and parallel two-stage evaporation vapor compression refrigeration cycle. *Energy Rep.* **2021**, *7*, 1616–1626. [CrossRef]
8. Lee, T.; Shin, K.-H.; Kim, J.; Jung, D.; Kim, J.-H. Design optimization of external variable displacement compressor with R1234yf for vehicle air conditioning system. *Appl. Therm. Eng.* **2021**, *198*, 117493. [CrossRef]
9. Guo, D.; Ma, Z.; Zhang, J.; Liu, M. Energy Impact of Air Pre-Cooling on Screw Air Compressor. *Procedia Eng.* **2017**, *205*, 937–944. [CrossRef]

10. Expósito-Carrillo, J.A.; Flor, F.J.S.L.; Perís-Pérez, B.; Salmerón-Lissén, J.M. Thermodynamic analysis of the optimal operating conditions for a two-stage CO_2 refrigeration unit in warm climates with and without ejector. *Appl. Therm. Eng.* **2021**, *185*, 116284. [CrossRef]
11. Jeon, Y.; Kim, S.; Kim, D.; Chung, H.J.; Kim, Y. Performance characteristics of an R600a household refrigeration cycle with a modified two-phase ejector for various ejector geometries and operating conditions. *Appl. Energy* **2017**, *205*, 1059–1067. [CrossRef]
12. Buffington, R.M.; Golkey, W. The thermodynamic properties of dichlorodifluormethane, a new refrigerant. *Ind. Eng. Chem.* **1931**, *23*, 254–256. [CrossRef]
13. Hendricks, J.O. Industrial fluorochemicals. *Ind. Eng. Chem.* **1953**, *45*, 99–105. [CrossRef]
14. Sokolov, M.; Hershgal, D. Enhanced ejector refrigeration cycles powered by low grade heat. Part 3. Experimental results. *Int. J. Refrig.* **1991**, *14*, 24–31. [CrossRef]
15. Velders, G.J.; Fahey, D.W.; Daniel, J.S.; McFarland, M.; Andersen, S.O. The large contribution of projected HFC emissions to future climate forcing. *Proc. Natl. Acad. Sci. USA* **2009**, *106*, 10949–10954. [CrossRef] [PubMed]
16. Velders, G.J.; Fahey, D.W.; Daniel, J.S.; Andersen, S.O.; McFarland, M. Future atmospheric abundances and climate forcings from scenarios of global and regional hydrofluorocarbon (HFC) emissions. *Atmos. Environ.* **2015**, *123*, 200–209. [CrossRef]
17. *Montreal Protocol: Montreal Protocol on Substances That Deplete the Ozone Layer*; US Government Printing Office: Washington, DC, USA, 1987; 26, pp. 128–136.
18. Carpenter, L.J.; Reimann, S.; Burkholder, J.B.; Clerbaux, C.; Hall, B.D.; Hossaini, R.; Laube, J.C.; Yvon-Lewis, S.A.; Engel, A.; Montzka, S.; et al. Update on ozone-depleting substances (ODSs) and other gases of interest to the Montreal protocol. *Sci. Assess. Ozone Deplet.* **2014**, *2014*, 1.
19. Linton, J.; Snelson, W.; Hearty, P. Performance comparison of refrigerants R-134a and R-12 in a residential exhaust air heat pump. *ASHRAE Trans. (Am. Soc. Heat. Refrig. Air-Cond. Eng.) (USA)* **1989**, *95*.
20. Lee, Y.; Su, C. Experimental studies of isobutane (R600a) as the refrigerant in domestic refrigeration system. *Appl. Therm. Eng.* **2002**, *22*, 507–519. [CrossRef]
21. Akintunde, M. Experimental investigation and modeling of moisture solubility in R12 and R134a. *J. Eng. Appl. Sci.* **2006**, *1*, 14–18.
22. *Regulation (EU) No 517/2014: Regulation (EU) No 517/2014 of the European Parliament and the Council of 16 April 2014 on fluorinated greenhouse gases and repealing Regulation (EC) No 842/2006*; Official Journal of the European Union: Maastricht, The Netherlands, 2014; p. 57.
23. Bolaji, B. Experimental study of R152a and R32 to replace R134a in a domestic refrigerator. *Energy* **2010**, *35*, 3793–3798. [CrossRef]
24. Kim, M.-H.; Lim, B.-H.; Chu, E.-S. The performance analysis of a hydrocarbon refrigerant R-600a in a household refrigerator/freezer. KSME International Journal. *KSME Int. J.* **1998**, *12*, 753–760. [CrossRef]
25. Joybari, M.M.; Hatamipour, M.S.; Rahimi, A.; Modarres, F.G. Exergy analysis and optimization of R600a as a replacement of R134a in a domestic refrigerator system. *J. Refrig.* **2013**, *36*, 1233–1242. [CrossRef]
26. Aprea, C.; Greco, A.; Maiorino, A.; Masselli, C.; Metallo, A. HFO1234ze as drop-in replacement for R134a in domestic refrigerators: An environmental impact analysis. *Energy Procedia* **2016**, *101*, 964–971. [CrossRef]
27. Lemmon, E.; Bell, I.H.; Huber, M.; McLinden, M. NIST Standard Reference Database 23: Reference Fluid Thermodynamic and Transport Properties-REFPROP, Version 10.0, National Institute of Standards and Technology. Standard Reference Data Program Gaithersburg. 2018.
28. Zilio, C.; Brown, J.; Schiochet, G.; Cavallini, A. The refrigerant R1234yf in air conditioning systems. *Energy* **2011**, *36*, 6110–6120. [CrossRef]
29. Navarro-Esbrí, J.; Mendoza-Miranda, J.; Mota-Babiloni, A.; Barragán-Cervera, A.; Belman-Flores, J. Experimental analysis of R1234yf as a drop-in replacement for R134a in a vapor compression system. *Int. J. Refrig.* **2013**, *36*, 870–880. [CrossRef]
30. Sánchez, D.; Cabello, R.; Llopis, R.; Arauzo, I.; Catalán-Gil, J.; Torrella, E. Energy performance evaluation of R1234yf, R1234ze(E), R600a, R290 and R152a as low-GWP R134a alternatives. *Int. J. Refrig.* **2017**, *74*, 269–282. [CrossRef]
31. Mota-Babiloni, A.; Navarro-Esbrí, J.; Barragán-Cervera, Á.; Molés, F.; Peris, B. Analysis based on EU Regulation No 517/2014 of new HFC/HFO mixtures as alternatives of high GWP refrigerants in refrigeration and HVAC systems. *Int. J. Refrig.* **2015**, *52*, 21–31. [CrossRef]
32. Devecioğlu, A.; Oruç, V. An analysis on the comparison of low-GWP refrigerants to alternatively use in mobile air-conditioning systems. *Therm. Sci. Eng. Prog.* **2017**, *1*, 1–5. [CrossRef]
33. Bull, J.; Buick, J.; Radulovic, J. Investigation of working fluid performance in a refrigeration cycle: A theoretical approach. In Proceedings of the 15th International Conference on Heat Transfer, Fluid Mechanics and Thermodynamics and Editorial Board of Applied Thermal Engineering: ATE-HEFAT 2021, Africa Massive, Midrand, South Africa, 25–28 July 2021; 2021.
34. Dewar, B.; Tiainen, J.; Jaatinen-Värri, A.; Creamer, M.; Dotcheva, M.; Radulovic, J.; Buick, J.M. CFD modelling of a centrifugal compressor with experimental validation through radial diffuser static pressure measurement. *Int. J. Rotating Mach.* **2019**, *2019*. [CrossRef]
35. Menter, F.R. Two-Equation Eddy-Viscosity Turbulence Models for Engineering Applications. *Am. Inst. Aeronaut. Astronaut. J.* **1994**, *32*, 1598–1605. [CrossRef]
36. Gibson, L.; Galloway, L.; Spence, S. Assessment of turbulence model predictions for a centrifugal compressor simulation. *J. Glob. Power Propuls. Soc.* **2017**, *1*, 142–156. [CrossRef]